Novel Route To Synthesize Complex Metal Sulfides: Hydrothermal Coupled Dissolution−Reprecipitation Replacement Reactions

Fang Xia,[†] Jinwen Zhou,[‡,⊥] Joël Brugger,[‡,§] Yung Ngothai,[†] Brian O'Neill,[†]
Guorong Chen,[||] and Allan Pring*[,‡,⊥]

School of Chemical Engineering and School of Earth and Environmental Sciences, University of Adelaide, Adelaide, SA 5005, Australia, Department of Mineralogy, South Australian Museum, Adelaide, SA 5000, Australia, Key Laboratory for Ultrafine Materials of Ministry of Education, School of Materials Science and Engineering, East China University of Science and Technology, Shanghai 200237, China, and School of Chemistry, Physics and Earth Sciences, The Flinders University of South Australia, GPO Box 2100, Adelaide, SA 5001, Australia

Received November 29, 2007. Revised Manuscript Received January 31, 2008

A novel route for the synthesis of complex metal sulfides using hydrothermal coupled dissolution−reprecipitation reactions is reported. Two thiospinels, $(Ni,Fe)_3S_4$ (violarite) and Co_3S_4 (linnaeite), were synthesized using $(Fe,Ni)_9S_8$ (pentlandite) and Co_9S_8 (cobaltpentlandite) as precursors. The Fe/Ni ratio of $(Ni,Fe)_3S_4$ can be adjusted by varying the reaction conditions, for example, temperature (125–145 °C), pH (2.90, 3.90, 5.00), and precursor stoichiometry ($(Fe_xNi_{1-x})_9S_8$, $x = 0.4, 0.5, 0.55, 0.6$). Pure $(Ni,Fe)_3S_4$ can be synthesized by utilizing a flow-through hydrothermal cell rather than a static hydrothermal cell as the fluid flow improves mass transfer and flushes away the Fe_2O_3 byproduct from the reaction front. Synthesis times range from 10 to 20 days, compared to the traditional dry synthesis route for $(Ni,Fe)_3S_4$ that requires 3 months annealing to obtain a product of only 72 ± 3 wt % purity. This synthesis route is ideal for preparing compounds with low thermal stabilities (<500 °C).

1. Introduction

Metal sulfides are of considerable interest in applied physics for their electrical and magnetic properties.[1] In particular, thiospinels have attracted growing attention for their magnetic, semiconducting and superconducting properties as well as the metal–insulator transitions exhibited by some compositions.[2–7] Syntheses of thiospinels are thus important to facilitate full characterization of their physical, chemical, and thermodynamic properties, and to the development of their potential magnetic and electrical applications.[1]

Many metal sulfides can be readily synthesized by the traditional dry condition method: heating the metal with elemental sulfur to high temperatures (>500 °C) in an evacuated sealed silica tube.[8] Others, however, are much more difficult to produce by this route because they have low thermal stabilities (<500 °C), and must be prepared at temperatures below their decomposition points. One such compound is the thiospinel mineral violarite (Vo), $(Ni,Fe)_3S_4$ (the ideal composition is $FeNi_2S_4$), which breaks down at 373 °C.[8] The main limitation of applying the traditional route to the synthesis of $(Ni,Fe)_3S_4$ is the slow reaction rate: several months annealing at or below 300 °C are required. Even then, the product always contains significant quantities of impurity phases such as nickeliferous pyrite $(Fe,Ni)S_2$.[9,10]

Other routes for the synthesis of metal sulfides have been developed in the last two decades, including the room temperature or mild hydrothermal solution routes,[11–15] gas–solid phase reactions,[16,17] or mechanical mixing.[18–20] Although various metal sulfides have been successfully synthesized by these methods, the products are largely restricted

---

* Corresponding author. Address: South Australian Museum. Tel.: +61 8 82077449. Fax: +61 8 82077222. E-mail: pring.allan@saugov.sa.gov.au.
† School of Chemical Engineering, University of Adelaide.
‡ South Australian Museum.
§ School of Earth and Environmental Sciences, University of Adelaide.
|| East China University of Science and Technology.
⊥ The Flinders University of South Australia.

(1) Pearce, C. I.; Pattrick, R. A. D.; Vaughan, D. J. *Rev. Mineral. Geochem.* **2006**, *61*, 127–180.
(2) Bitoh, T.; Hagino, T.; Seki, Y.; Chikazawa, S.; Nagata, S. *J. Phys. Soc. Jpn.* **1992**, *61*, 3011–3012.
(3) Hagino, T.; Seki, Y.; Wada, N.; Tsuji, S.; Shirane, T.; Kumagai, K.; Nagata, S. *Phys. Rev. B* **1995**, *51*, 12673–12684.
(4) Nagata, S.; Matsumoto, N.; Kato, Y.; Furubayashi, T.; Matsumoto, T.; Sanchez, J. P.; Vulliet, P. *Phys. Rev. B* **1998**, *58*, 6844–6854.
(5) Sugita, H.; Wada, S.; Yamada, Y.; Miyatani, K.; Tanaka, T. *J. Phys. Soc. Jpn.* **1998**, *67*, 1401–1408.
(6) Park, M. S.; Kwon, S. K.; Min, B. I. *Phys. Rev. B* **2001**, *64*, 100403.
(7) Fang, L.; Zou, P. Y; Lu, X. F.; Xu, Z.; Chen, H.; Shan, L.; Wen, H. H. *Phys. Rev. B* **2005**, *71*, 064505.
(8) Vaughan, D. J.; Craig, J. R. *Mineral chemistry of metal sulfides*; Cambridge University Press: Cambridge, 1978.
(9) Craig, J. R. *Am. Mineral.* **1971**, *56*, 1303–1311.
(10) Tenailleau, C.; Etschmann, B.; Ibberson, R. M.; Pring, A. *Am. Mineral.* **2006**, *91*, 1442–1447.
(11) Magafas, L.; Anagnostopoulos, A. N.; Antonopoulos, J. G. *Phys. Status Solidi A* **1989**, *111*, K175–K178.
(12) Wang, C.; Zhang, X.; Qian, X.; Wang, W.; Qian, Y. *Mater. Res. Bull.* **1998**, *33*, 1083–1086.
(13) Jeong, Y. U.; Manthiram, A. *Inorg. Chem.* **2001**, *40*, 73–77.
(14) Shimizu, Y.; Yano, T. *Chem. Lett.* **2001**, *20*, 1028–1029.
(15) Liu, X. *Mater. Sci. Eng., B* **2005**, *119*, 19–24.
(16) Tenne, R.; Margulis, L.; Genut, M.; Hodes, G. *Nature* **1992**, *360*, 444–446.
(17) Nath, M.; Govindaraj, A.; Rao, C. N. R. *Adv. Mater.* **2001**, *13*, 283–286.
(18) Kosmac, T.; Maurice, D.; Courtney, T. H. *J. Am. Ceram. Soc.* **1993**, *76*, 2345–2352.
(19) Baláž, P.; Havlík, T.; Bastl, Z.; Brianěin, J. *J. Mater. Sci. Lett.* **1995**, *14*, 344–346.
(20) Baláž, P.; Havlík, T.; Brianěin, J.; Kammel, R. *Scr. Metall. Mater.* **1995**, *32*, 1357–1362.

10.1021/cm7033883 CCC: $40.75

Table 1. Summary of the Starting Compositions and Chemistry of Synthesized Precursors[a]

	starting composition (atom %)							
precursor code	Fe	Ni	Co	S	precursor stoichiometry	Fe/Ni ratio	unit cell dimension (Å)	impurities
Pn1	20.86	32.52		46.62	$Fe_{3.62}Ni_{5.39}S_8$	0.67(1)	10.1046(1)	α-(Fe,Ni), Ni_3S_2
Pn2	26.69	26.69		46.62	$Fe_{4.60}Ni_{4.55}S_8$	1.01(1)	10.1158(1)	Ni_3S_2
Pn3	29.60	23.78		46.62	$Fe_{5.08}Ni_{3.98}S_8$	1.28(1)	10.1337(1)	Ni_3S_2
Pn4	32.52	20.86		46.62	$Fe_{5.61}Ni_{3.46}S_8$	1.62(1)	10.1624(1)	Ni_3S_2
Cpn1			52.94	47.06	$Co_{8.96}S_8$		9.9263(1)	$Co_{1-x}S$, Co

[a] Note: Impurities Ni_3S_2, $Co_{1-x}S$, and Co are easy to avoid in the products (see text for detail).

to relatively simple compounds, such as Ag_2S, NiS, CdS, FeS, and ZnS, and most of the products synthesized are either poorly crystallized or contain impurities.

Sulfide minerals are the major ores of many metals, including Pb, Ag, Co, Ni, Cu, and Zn. In Nature, these minerals are often deposited not from melts, but from hydrothermal aqueous fluids at temperatures between 50 and 500 °C and at pressures from 0.1 to >200 MPa. In low-temperature systems (<250 °C), the sulfide minerals often form by replacing an existing mineral, a mineralogical process known as pseudomorphism. Such reactions can occur at temperatures as low as 30 °C in the upper parts of ore deposits and even on ore dumps and during ore processing. Understanding the natural processes of replacement reactions in sulfide minerals provides insights into new ways of synthesizing mixed metal sulfides, such as thiospinels.

As part of a wider study into the mechanisms and kinetics of replacement reactions in sulfide minerals we investigated the transformation of pentlandite $(Fe,Ni)_9S_8$ (space group $Fm\bar{3}m$), formed by exsolution from Ni-bearing pyrrhotite, to violarite $(Ni,Fe)_3S_4$ (space group $Fm\bar{3}m$) under hydrothermal conditions.[21,22] We noted that the transformation was relatively rapid at 120 °C (3 days) and it occurred to us that these hydrothermal replacement reactions might be an effective route to synthesize mixed metal sulfides of low thermal stabilities. We report here details of the successful synthesis of pure $(Ni,Fe)_3S_4$ and Co_3S_4 (linnaeite) via this route. Co_3S_4 possesses a relatively high thermal stability, decomposing at 664 °C,[8] and its synthesis demonstrates that this route is effective for synthesizing materials across a wide range of thermal stabilities. $(Fe,Ni)_9S_8$ (pentlandite) and Co_9S_8 (cobaltpentlandite) were utilized as precursors, as they can be prepared efficiently via the traditional dry silica-tube route. $(Ni,Fe)_3S_4$ was also synthesized by the traditional route for a direct comparison of the purity and grain size of the products. In this paper, $(Ni,Fe)_3S_4$ synthesized by the hydrothermal method is denoted H-$(Ni,Fe)_3S_4$ and that by the traditional dry method D-$(Ni,Fe)_3S_4$.

2. Experimental Section

2.1. Hydrothermal Synthesis of H-$(Ni,Fe)_3S_4$ and Co_3S_4. The synthesis of $(Ni,Fe)_3S_4$ and Co_3S_4 via the hydrothermal replacement reaction route was a two-steps process: first preparation of the precursors $(Fe,Ni)_9S_8$ or Co_9S_8 by dry synthesis, followed by replacement via a coupled dissolution−reprecipitation replacement reaction under mild hydrothermal conditions. The precursors were synthesized by the standard silica-tube method.[23] High purity elemental Fe (1 mm diameter wire, 99.9+%, Aldrich), Ni (0.5 mm diameter wire, 99.9+%, Aldrich), Co (100 mesh powder, 99.9+% Aldrich), and S (flakes 99.99+%, Aldrich) were accurately weighed according to the compositions shown in Table 1 and sealed into 10 mm diameter silica tubes under vacuum (10^{-2} torr). Each 5 g charge was placed vertically in a muffle furnace and heated slowly (1 °C/min) to 445 °C, with subsequent heating to 700 °C, annealing for 3 h at each stage to minimize the tube failure due to high S vapor pressure. Following that, the charges were heated to 1150 °C and annealed for 10 h. Finally the furnace was turned off and the charges were allowed to cool to room temperature slowly overnight. Temperatures were controlled within an error range of ±2 °C during the syntheses. Pure pentlandite was generally obtained by removing a thin Ni_3S_2 coating on the products, but the Ni-rich composition $(Ni_{5.39}Fe_{3.62})S_8$ (Pn1) also retained small amounts of α-(Fe,Ni) after removal of the Ni_3S_2 coating. This impurity did not affect the purity of the H-$(Fe,Ni)_3S_4$ product. The stoichiometries and unit cell dimensions of the $(Fe,Ni)_9S_8$ precursors listed in Table 1 are in excellent agreement with published data.[24–26] During the synthesis of Co_9S_8, the melt separated into two parts upon cooling: the upper part of the pellet (~25 wt %) contained lamellar $Co_{1-x}S$ in a Co_9S_8 host, whereas the lower part was almost pure Co_9S_8, with a trace of Co metal noted in SEM examination but undetectable by X-ray diffraction (XRD). The lower part of the pellet was used as the precursor for Co_3S_4 synthesis and it was found that the trace of Co metal did not affect the purity of product. The bulk precursors were crushed and sieved, and the 400–1000 μm fractions were ultrasonically cleaned and used in the syntheses for H-$(Ni,Fe)_3S_4$ and Co_3S_4.

The hydrothermal replacement reactions were conducted at temperatures between 125 and 165 °C using a custom-built 316 stainless steel flow-though closed-loop hydrothermal cell (Figure 1). Fluid circulation was driven by thermosyphon: the fluid in the reservoir (150 mL) was heated by an electrical heating jacket and then cooled by a double-pipe heat exchanger on the other side of the loop. The flow rate was maintained within the range of 0.06 $m.s^{-1}$ to 0.08 $m.s^{-1}$. The precursor was loaded into a fine mesh (280 × 280 μm^2) 316 stainless steel tube, and placed into the flow-through reaction cell. In order to leave 50 mL free space for fluid expansion at the reaction temperature, 210 mL of solution was introduced in the reactor (total volume 260 mL). Hence the pressure of the system was near the liquid–vapor pressure of water. This air gap provides not only for fluid expansion but provides an oxygen supply, which serves as an oxidant for the reactions. The temperatures at the reservoir (T1), the heat exchanger (T2) and the

---

(21) Tenailleau, C.; Pring, A.; Etschmann, B.; Brugger, J.; Grguric, B. A.; Putnis, A. *Am. Mineral.* **2006**, *91*, 706–709.

(22) Xia, F.; Zhou, J.; Pring, A.; Ngothai, Y.; O'Neill, B.; Brugger, J.; Chen, G.; Colby, C. *React. Kinet. Catal. Lett.* **2007**, *92*, 257–266.

(23) Drebushchak, V. A.; Kravchenko, T. A.; Pavlyuchenko, V. S. *J. Cryst. Growth* **1998**, *193*, 728–731.

(24) Knop, O.; Ibrahim, M. A.; Sutarno, R. *Can. Mineral.* **1965**, *8*, 291–316.

(25) Chamberlain, A. C. *The effect of stoichiometry on the thermal behaviour of synthetic iron-nickel sulfides*; Curtin University of Technology: Perth, 1996.

(26) Etschmann, B.; Pring, A.; Putnis, A.; Grguric, B. A.; Studer, A. *Am. Mineral.* **2004**, *89*, 39–50.

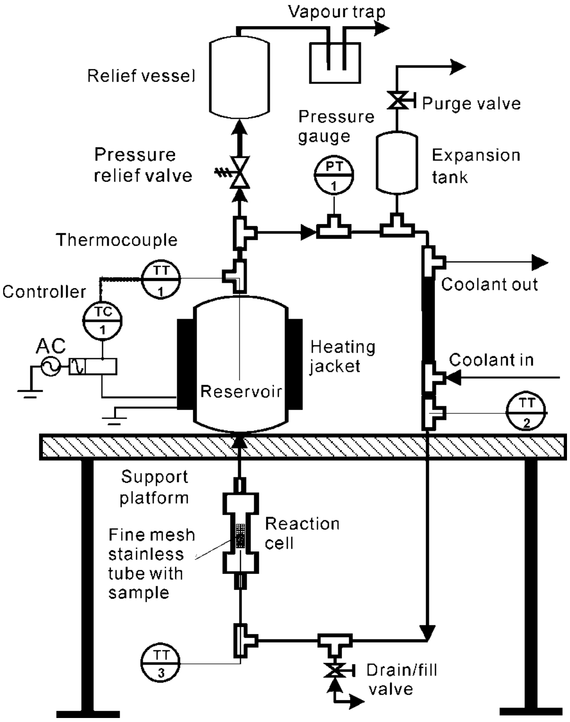

Figure 1. Schematic diagram of the 316 stainless steel thermosyphon driven flow-through hydrothermal cell. The volume of the reservoir, the expansion tank, and the cell are 150 mL, 75 mL, and 25 mL, respectively. The total internal volume of the cell, including tubing, is 260 mL.

reaction site (T3; this is the reaction temperature listed in Table 2) were monitored by thermocouples (T1 > T2 > T3). The temperature in the reservoir is between 10 and 20 °C higher than T3. The reaction was interrupted at intervals (usually every 24 h) for replacement of the fluid with a fresh buffer solution. This also enabled the air in the expansion tank to be replaced and the removal of a small part of the sample for analysis by XRD, SEM, and EMP. A range of experimental conditions, summarized in Table 2, was used to study the effects of pH, temperature, and $(Fe,Ni)_9S_8$ precursor composition on the chemistry of the H-$(Ni,Fe)_3S_4$ product. The solutions consist of 0.2 m H_3PO_4/NaH_2PO_4 or CH_3COOH/CH_3COONa pH buffers prepared using deionized water and resulting in $pH_{25\ °C}$ of 2.90, or 3.90 and 5.00, respectively. These pH conditions were selected as $(Fe,Ni)_9S_8$ and $(Ni,Fe)_3S_4$ become unstable below pH 1.[21] Warner et al. attempted to convert $(Fe,Ni)_9S_8$ to $(Ni,Fe)_3S_4$ in a very acidic solution (pH = 0) at 80 °C, but formed only some elemental sulfur.[27] The $(Fe,Ni)_9S_8$ precursors were also transformed to H-$(Ni,Fe)_3S_4$ in a 260 mL static cell lined with Teflon under the same reaction conditions, in order to probe the effects of fluid flow. Several samples of H-$(Fe,Ni)_3S_4$ were annealed in evacuated sealed silica tubes at 300 °C for up to 33 days in order to study the variations in crystallite size, cell dimension and phase stability. These were also used for comparison with the products of dry synthesis, (D-$(Fe,Ni)_3S_4$).

The $Co_9S_8$was transformed to Co_3S_4 at pH 3.90 and at 165 °C in the flow-through reactor.

2.2. Synthesis of D-$(Fe,Ni)_3S_4$ (Dry Conditions). Four $(Fe_{1-x}Ni_x)_3S_4$ compositions with different Fe/Ni ratios were synthesized (Table 3). Elemental Fe, Ni, and S (as per the synthesis of $(Fe,Ni)_9S_8$) were accurately weighed to give *mss* (monosulfide solid solution) compositions $Fe_xNi_{1-x}S$ (x = 0.25, 0.33, 0.4, 0.5) and sealed into silica tubes under vacuum. The charges were heated slowly (as per pentlandite syntheses) to 1000 °C and annealed for 2 days, then cooled to 900 °C and annealed for a further 7 days. The charges were then quenched in cold water. The products were checked by XRD and were confirmed as pure *mss*. The *mss* was ground to powder, then sulfur was added to yield the desired nominal stoichiometries, and the mixture was sealed in new silica tubes. The charges were annealed at 300 °C for 20 days and then quenched in cold water. To achieve purer D-$(Ni,Fe)_3S_4$, the products were reground, sealed inside new silica tubes, and annealed for another 80 days at 300 °C.

2.3. Analytical Methods. The phases were identified by room temperature powder XRD, using a Huber image plate Guinier Camera with Co $K\alpha_1$ radiation (λ = 1.78892 Å). The samples were ground in acetone, spread uniformly on a MYLAR film, and then mounted on the sample oscillation unit for data collection.

The phase fractions and cell dimensions were determined by Rietveld Quantitative Phase Analysis (RQPA) using Rietica for Windows (v1.7.7).[28] Small, accurately weighed amounts of NBS Si were added as internal standard to some samples. For samples measured without Si, the zero shifts for the refinement procedures were taken from refinements using the NBS external Si standard. For each XRD data set, the background and phase fraction were refined first, followed by unit cell parameters, and finally peak-shape parameters. The background was modeled using a fifth order polynomial, and peak shape using pseudo-Voigt (Howard Asymmetry). The initial structural models of $(Fe,Ni)_9S_8$, *mss*, ferroan millerite (Ni,Fe)S, $(Ni,Fe)_3S_4$, Co_9S_8, Co_3S_4, and $(Fe,Ni)S_2$ were derived from literature.[29–35]

The crystallite size of $(Ni,Fe)_3S_4$ was calculated from the Full Width at Half Maximum (FWHM) broadening of the (113) reflection in the XRD patterns. The instrumental FWHM curve was calibrated using a NBS Si standard: the instrumental FWHM at the $(111)_{Si}$ reflection is 0.160°. The crystallite sizes were then calculated using the Scherrer formula:

$$\text{Crystallite size} = \frac{K\lambda}{\beta\cos(\theta)} \qquad (1)$$

where θ is the peak position, K is the shape factor of the average crystallite, which was set to 0.89 in this calculation (assuming the crystallites are spherical), λ refers to the wavelength (nm) of the X-ray radiation, and β is the specimen broadening from the instrumental FWHM value of a peak.

The SEM images were obtained using a Philips XL30 field emission scanning electron microscope (FESEM). Surface morphology and cross-sections were imaged in secondary and backscattered electron modes, respectively. Acceleration voltages of either 15 kV or 20 kV were used depending on the samples to optimize contrast or resolution.

The chemical composition of the samples was determined using a CAMEBAX SX51 electron microprobe (EMP). The analyses were undertaken using an accelerating potential of 20 kV and a specimen current of ~20 nA. The spot size was set at 1 μm but the effective resolution of the beam due to beam spread in the sample was of

---

(27) Warner, T. E.; Rice, N. M.; Taylor, N. *Hydrometallurgy* **1992**, *31*, 55–90.

(28) Hunter, B. A. *Int. Union Crystallogr. Comm. Powder Diffr. Newslett.* **1998**, *20*, 21–23.

(29) Pearson, A. D.; Buerger, M. J. *Am. Mineral.* **1956**, *41*, 804–805.

(30) Alsen, N. *Geologiska Foereningens i Stockholm Foerhandlingar* **1925**, *47*, 19–73.

(31) Rajamani, V.; Prewitt, C. T. *Can. Mineral.* **1974**, *12*, 253–257.

(32) Vaughan, D. J.; Craig, J. R. *Am. Mineral.* **1985**, *70*, 1036–1043.

(33) Rajamani, V.; Prewitt, C. T. *J. Solid State Chem.* **1976**, *16*, 97–116.

(34) Knop, O.; Reid, K. I. G.; Sutarno, R.; Nakagawa, Y. *Can. J. Chem.* **1968**, *46*, 3463–3476.

(35) Wu, R.; Zheng, Y. F.; Zhang, X. G.; Sun, Y. F.; Xu, J. B.; Jian, J. K. *J. Cryst. Growth* **2004**, *266*, 523–527.

Table 2. Summary of the Reaction Conditions and Chemistry of Products Synthesized Using the Coupled Dissolution−Reprecipitation Route

expt. code	precursor	$pH_{25\,°C}$[a]	T[b] (°C)	time (day)	product stoichiometry[c]	M/S	Fe/Ni	unit cell dimension (Å) As prepared	 300 °C 33 days
HV1	Pn2	2.90	125	16	$Fe_{1.45}Ni_{1.45}S_4$	0.725(2)	1.00(1)	9.4881(1)	9.4727(1)
HV2	Pn2	3.90	125	7	$Fe_{1.19}Ni_{1.77}S_4$	0.740(2)	0.67(1)	9.4858(1)	9.4706(1)
HV3	Pn2	5.00	125	6[d]	$Fe_{1.05}Ni_{1.87}S_4$	0.730(2)	0.56(1)	9.4837(1)	9.4709(1)
HV4	Pn2	3.90	135	14	$Fe_{1.04}Ni_{1.95}S_4$	0.748(2)	0.53(1)	9.4740(1)	9.4687(1)
HV5	Pn2	3.90	145	20	$Fe_{0.91}Ni_{2.05}S_4$	0.740(2)	0.44(1)	9.4841(1)	
HV6	Pn1	3.90	125	12	$Fe_{1.05}Ni_{1.93}S_4$	0.745(2)	0.54(1)	9.4863(1)	
HV7	Pn3	3.90	125	9	$Fe_{1.69}Ni_{1.35}S_4$	0.760(2)	1.25(1)	9.4816(1)	
HV8	Pn4	3.90	125	20	$Fe_{1.86}Ni_{1.24}S_4$	0.775(2)	1.50(1)	9.4780(1)	
HL1	Cpn1	3.90	165	10	$Co_{2.75}S_4$	0.688(2)		9.4110(1)	

[a] pH 2.90 was controlled by $H_3PO_4 + NaH_2PO_4$ pH buffer, pH 3.90 and 5.00 were controlled by $CH_3COOH + CH_3COONa$ pH buffer. [b] These temperatures correspond to temperatures T_3 in the text. [c] The stoichiometries are the mean values of at least 10 points measurements by EMP analysis. [d] After 6 days, the reaction stalls at ~35% completion, the reason remains unclear.

Table 3. Summary of the Starting Compositions and Chemistry of D-$(Ni,Fe)_3S_4$ Synthesized Using the Traditional Dry Route

expt. code	batch compositions (atom %) Fe	 Ni	 S	D-$(Ni,Fe)_3S_4$ stoichiometry	unit cell dimension (Å)	M/S	Fe/Ni	purity (wt %)	impurities[a]
DV1	10.72	32.14	57.14	$Fe_{0.95}Ni_{2.01}S_4$	9.4601(1)	0.740(2)	0.47(1)	70(3)	Ml, *mss*
DV2	14.27	28.59	57.14	$Fe_{0.94}Ni_{2.04}S_4$	9.4624(1)	0.745(2)	0.46(1)	73(3)	Ml, *mss*, Py
DV3	17.14	25.72	57.14	$Fe_{1.31}Ni_{1.58}S_4$	9.4726(1)	0.723(2)	0.83(1)	62(3)	*mss*, Py
DV4	21.43	21.43	57.14	Vo1:$Fe_{1.79}Ni_{1.40}S_4$	9.4736(1)	0.798(2)	1.28(1)	54(3)	*mss*, Py
				Vo2:$Fe_{0.44}Ni_{2.34}S_4$	9.4748(1)	0.695(2)	0.19(1)		

[a] Ml stands for (Ni,Fe)S (space group $R3m$), *mss* for (Ni,Fe)S (space group $P6_3/mmc$), and Py for $(Fe,Ni)S_2$ (space group $Pa\bar{3}$).

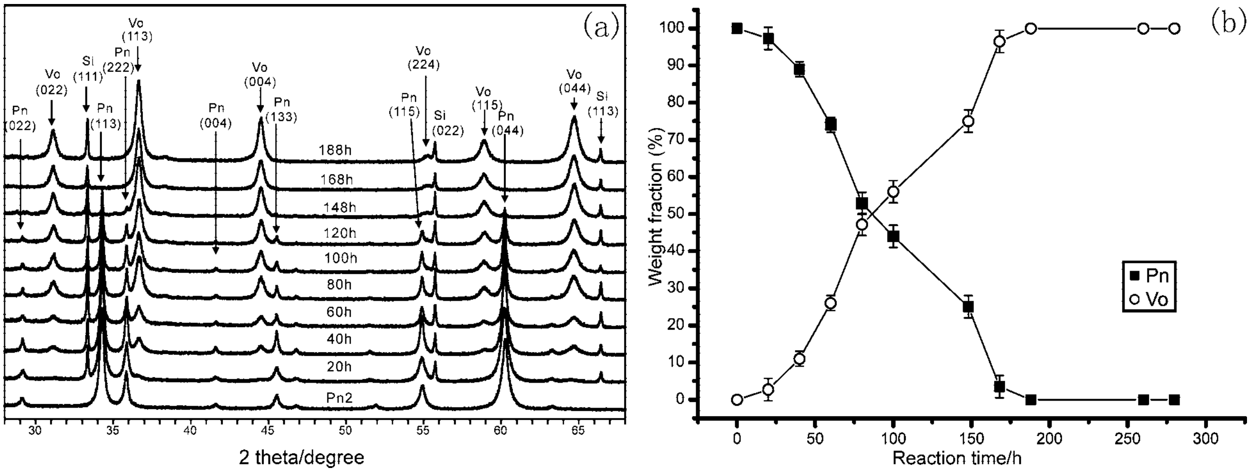

Figure 2. (a) Stack of powder X-ray diffraction patterns showing the progress of H-$(Ni,Fe)_3S_4$ synthesis by hydrothermal replacement of $Fe_{4.60}Ni_{4.55}S_8$ at 125 °C and pH 3.90. (b) The weight fraction of phases against reaction time obtained by least-squares Rietveld refinement of XRD data from (a). Symbol Pn stands for precursor $Fe_{4.60}Ni_{4.55}S_8$, Vo for product H-$(Ni,Fe)_3S_4$, and Si for NBS silicon standard.

the order of 3 μm. Natural pentlandite (Astimex #36) and cobaltite (Astimex #19) were used as standards for Fe, Ni, and S, and Co, respectively.

3. Results and Discussion

3.1. Reaction Mechanism for H-$(Ni,Fe)_3S_4$ Synthesis. The main precursor composition used in this study, $(Fe_{4.6}Ni_{4.55})S_8$ (Pn2), was selected because it approaches the most stable pentlandite stoichiometry ($Fe_{4.5}Ni_{4.5}S_8$).[36] The progress of the transformation was monitored by RQPA. Figure 2 shows the stack of XRD patterns and the weight fraction changes with reaction time for the transformation of Pn2 to H-$(NiFe)_3S_4$ at 125 °C and pH 3.90. This transformation took approximately 7 days to complete. The reaction conditions, transformation time, product stoichiometries and unit cell dimensions are summarized in Table 2.

The progress of the transformation can also be monitored using backscattered electron images taken from cross sections of grains removed from the reaction at different stages of the experiment (Figure 3). The reaction commences at the outer surface of the precursor and generates both large- and fine-scale cracks. The reaction front proceeds toward the core of the grains mainly via the large cracks. Sharp reaction fronts were observed for all reaction conditions (Figure 3d,f).

For many years it was thought that replacement reactions of this kind were driven and controlled by solid-state diffusion of the metal ions through the minerals.[37] However, Putnis and coauthors have recently suggested that many mineral replacements are in fact the product of coupled dissolution and reprecipitation reactions, with a hydrothermal fluid transporting metals and other elements to and from the reaction front, rather than a solid-state diffusion process.[38–42]

---

(36) Burdett, J. K.; Miller, G. J. *J. Am. Chem. Soc.* **1987**, *109*, 4081–4091.

(37) Cole, D. R.; Chakraborty, S. *Rev. Mineral. Geochem.* **2001**, *43*, 82–223.

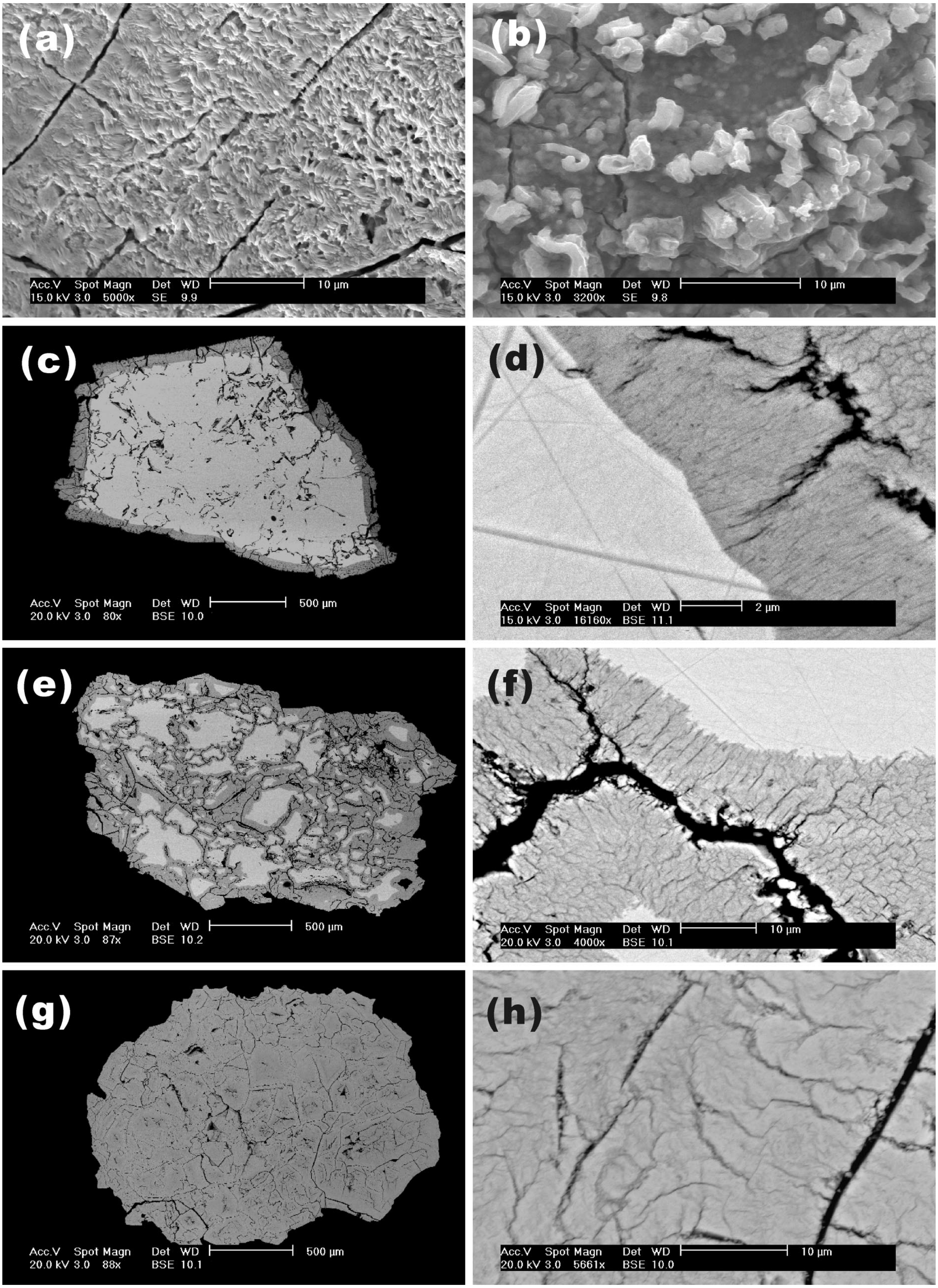

Figure 3. Selected SEM micrographs of reacted samples using precursor Pn2 ($Fe_{4.60}Ni_{4.55}S_8$). (a) and (b) are the secondary electron (SE) micrographs for the surface morphology of samples during the mid stage of reactions using the flow-through cell and the static Teflon inner hydrothermal cell, respectively. Note that in (b) Fe_2O_3 particles (white) are observed on the surface. (c−h) Backscattered electron (BSE) micrographs: (c) a partially reacted grain at 125 °C and pH 3.90, (d) the enlargement of the reaction front from (c), (e) a partially reacted grain at 145 °C and pH 3.90, (f) the enlargement of the reaction front from (e), (g) a completely reacted grain at 145 °C and pH 3.90, and (h) an enlargement from the center of (g). In these BSE images, the bright and grey regions are unreacted precursor and synthetic H-$(Ni,Fe)_3S_4$, respectively.

This mechanism is strongly supported by isotope studies, where the ^{18}O present in solution was found within the product structure, indicating the destruction of the whole precursor structure before forming the products.[41,43,44] In all these transformations, the porous and finely cracked texture of the product provides pathways for enhanced fluid and mass flow to and from the reaction front. The distinctive features of the replacement reaction from $(Fe,Ni)_9S_8$ to $(Ni,Fe)_3S_4$ are consistent with a coupled dissolution−reprecipitation pathway rather than a solid-state diffusion controlled mechanism as the sharp reaction front implies little or no compositional gradient that is common in solid-state diffusion reactions, and cracks are rarely produced by solid-state diffusion reactions. Furthermore, the kinetics of a solid-state diffusion controlled process should increase with reaction temperature, but our experimental data show that the rate deceases to one-third when the temperature is increased from 125 to 145 °C (Table 2), and the fluid chemistry has a first order effect on reaction kinetics, which is not expected for a solid-state reaction. Finally, attempts to synthesize $FeNi_2S_4$ via a solid-state diffusion reaction by reacting $(Fe,Ni)_9S_8$ with $Fe_{1-x}S$ or S at 300 °C were not successful.[45]

The porous texture appears to be mostly related to the volume contraction of around 18% when transforming from $(Fe,Ni)_9S_8$ to H-$(Ni,Fe)_3S_4$, releasing excess Fe^{2+} and Ni^{2+} ions. The highly insoluble Fe_2O_3 was not detected in the H-$(Ni,Fe)_3S_4$ product from the flow-through experiments (as opposed to the closed-cell experiments where Fe_2O_3 precipitated both onto the H-$(Ni,Fe)_3S_4$ product and the Teflon cell wall), but formed a slurry in the residual fluid. This suggests that Fe dissolves as Fe^{2+}, is carried away in the fluid, and is subsequently oxidized to Fe^{3+} which precipitates as insoluble Fe_2O_3.[46] The coupled dissolution−reprecipitation replacement from $(Fe,Ni)_9S_8$ to H-$(Ni,Fe)_3S_4$ can be tentatively described by the three following reactions:

$(Fe,Ni)_9S_8$ dissolution:

$$Fe_xNi_{9-x}S_8 + 18H^+ + 0.5O_2(aq) = (9-x)Ni^{2+} + xFe^{2+} + 8H_2S(aq) + H_2O \quad (2)$$

H-$(Ni,Fe)_3S_4$ precipitation:

$$2yFe^{2+} + (6-2y)Ni^{2+} + O_2(aq) + 8H_2S(aq) = 2Fe_yNi_{3-y}S_4 + 12H^+ + 2H_2O \quad (3)$$

Reactions (2) and (3) are written assuming acidic, reducing conditions at the reaction front (Fe^{2+}, $H_2S(aq)$). Reactions (2) and (3) both are oxidation reactions, so it is clear that an oxidant is essential for H-$(Ni,Fe)_3S_4$ synthesis. The 50 mL air in the expansion tank provides extra O_2 by the continuous fluid flow when aqueous oxygen is consumed at the reaction site. If the O_2 in the expansion tank is not regularly replenished during the experimental run, the transformation stops after ~48 h.

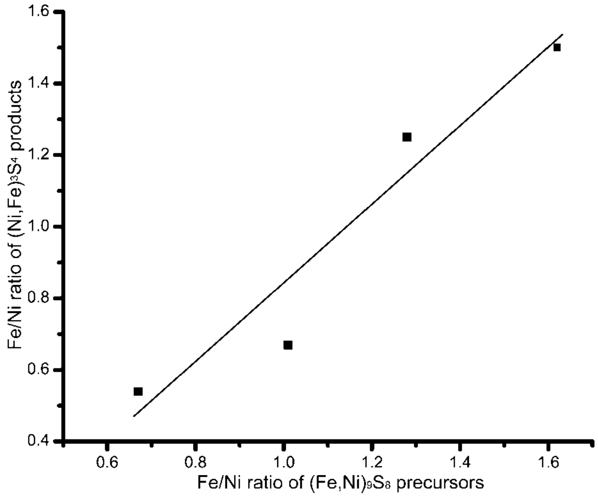

Figure 4. Plot of the correlation between the Fe/Ni ratios of precursor $(Fe,Ni)_9S_8$ and product H-$(Ni,Fe)_3S_4$. The straight line through the data points is the linear fit with R = 0.97 at 95% confidence level. The line can be expressed as $Fe/Ni_{product} = 1.09\ Fe/Ni_{precursor} - 0.26$.

Reactions (2) and (3) are tightly coupled, with the following reaction occurs away from the reaction front. The Fe_2O_3 in the equation was confirmed by XRD as hematite:

$$(x-2y)Fe^{2+} + (0.25x-0.5y)O_2(aq) + (2x-4y)OH^- = (0.5x-y)Fe_2O_3 + (x-2y)H_2O \quad (4)$$

The resulting overall reaction is

$$Fe_xNi_{9-x}S_8 + (6-2x+4y)H^+ + (1.5+0.25x-0.5y)O_2(aq) = 2Fe_yNi_{3-y}S_4 + (3-x+2y)Ni^{2+} + (0.5x-y)Fe_2O_3 + (3-x+2y)H_2O \quad (5)$$

3.2. Chemistry of Synthetic H-$(Ni,Fe)_3S_4$.

The metal to sulfur ratio (M/S) is relatively constant in all H-$(Ni,Fe)_3S_4$, but the Fe/Ni ratio depends on pH, temperature, and starting precursor stoichiometry (Table 2). For reactions at 125 °C using the most stable precursor Pn2 (HV1, HV2, HV3), the Fe/Ni ratio decreases significantly with increasing pH: 1.00 for pH 2.90, 0.67 for pH 3.90, and 0.56 for pH 5.00. The reason for this is probably related to the fact that Fe_2O_3 precipitation is favored by the higher pH, leaving a nickel rich solution accordingly. For reactions at pH 3.90 with precursor Pn2 (HV2, HV4, HV5), the Fe/Ni ratio decreases with increasing temperature: 0.67 at 125 °C, 0.53 at 135 °C, and 0.44 at 145 °C. This, again, may be explained by Fe_2O_3 precipitation affecting the Fe/Ni ratio in the fluid, because the solubility of Fe_2O_3 decreases with increasing temperature.[46,47] The stoichiometry of the precursor exerts the most significant influence on the stoichiometry of H-$(Ni,Fe)_3S_4$, and a strong correlation was found between the Fe/Ni ratio in the precursor and that of the product (Figure 4). Such correlation was also observed for natural pentlandite/violarite

---

(38) Putnis, A. *Mineral. Mag.* **2002**, *66*, 689–708.
(39) Putnis, C. V.; Mezger, K. *Geochim. Cosmochim. Acta* **2004**, *68*, 2839–2848.
(40) Putnis, C. V.; Tsukamoto, K.; Nishimura, Y. *Am. Mineral.* **2005**, *90*, 1909–1912.
(41) Putnis, C. V.; Geisler, T.; Schmid-Beurmann, P.; Stephan, T.; Giampaolo, C. *Am. Mineral.* **2007**, *92*, 19–26.
(42) Putnis, A.; Putnis, C. V. *J. Solid State Chem.* **2007**, *180*, 1783–1786.
(43) Labotka, T. C.; Cole, D. R.; Fayek, M.; Riciputi, L. R.; Stadermann, F. J. *Am. Mineral.* **2004**, *89*, 1822–1825.
(44) O'Neill, J. R.; Taylor, H. P. *Am. Mineral.* **1967**, *52*, 1414–1437.
(45) Yin, W.; Tenailleau, C.; Pring, A.; Brugger, J. In *Regolith 2004: Proceedings of the CRC LEME Regional Regolith Symposia*; Roach, I. C., Ed.; Cooperative Research Center for Landscape Environments and Mineral Exploration: Adelaide, Perth & Canberra, Australia, 2004; pp 146–150.
(46) Liu, W.; Etschmann, B.; Brugger, J.; Spiccia, L.; Foran, G.; Mclnnes, B. *Chem. Geol.* **2006**, *231*, 326–349.
(47) Diakonov, I. I.; Schott, J.; Martin, F.; Harrichourry, J. C.; Escalier, J. *Geochim. Cosmochim. Acta* **1999**, *63*, 2247–2261.

assemblages.[48] Again, this control by the chemistry of the pentlandite is interpreted as reflecting the Fe/Ni ratio in the fluid at the reaction front, and this appears to be controlled by nearly congruent dissolution of pentlandite. It seems that both bulk (e.g., bulk fluid pH) and local solution chemistry (e.g., composition of the material being replaced) affect the composition of the product. This provides great scope and flexibility for fine-tuning the composition of the product.

The unit cell dimensions of the H-$(Ni,Fe)_3S_4$ are in the range from 9.4740(1) Å to 9.4881(1) Å, similar to those reported $(Ni,Fe)_3S_4$.[32,10] Recent neutron diffraction studies on dry synthetic $(Ni,Fe)_3S_4$ indicate that it adopts the inverse spinel structure, where Ni occupies the tetrahedral sites and the low spin Fe with the remaining Ni adopts the octahedral sites.[10] It is not possible from the cell parameters alone to, determine whether H-$(Ni,Fe)_3S_4$ is an normal, inverse or disordered spinel. This would require the synthesis of samples prepared with isotopic ^{60}Ni and neutron diffraction studies to establish state of order. However, Tenailleau et al. attempted to disorder the inverse spinel structure of D-$(Ni,Fe)_3S_4$ over a large temperature range without success.[10]

The purity of H-$(Ni,Fe)_3S_4$ products was checked by XRD and EMP microchemical analyses. The XRD patterns of all synthetic H-$(Ni,Fe)_3S_4$ show no other phases. The line scans of EMP analyses indicate that the products are quite homogeneous even though the weight fractions of the three elements (Fe, Ni, S) change from point to point within small ranges (±1.2%). However, when the static Teflon lined hydrothermal cell was used, Fe_2O_3 precipitated within the larger cracks and on grain surfaces (Figure 3b), and the reaction rate slowed. This is because the fluid flow in the flow-through cell not only favors the reaction by accelerating the mass transfer between the reaction front and the bulk fluid, but also flushes away excess Fe^{2+} before it can oxidize to Fe^{3+}, nucleate and grow onto the product. Fe_2O_3 is difficult to remove, thus the static hydrothermal cell may not be suitable for synthesis of pure H-$(Ni,Fe)_3S_4$.

3.3. Effect of Further Annealing at 300 °C on H-$(Ni,Fe)_3S_4$. To study the effect of annealing, a few synthetic H-$(Ni,Fe)_3S_4$ samples were heated at 300 °C for up to 33 days in evacuated silica tubes. It was found that the unit cell contracted upon annealing (Table 2). The cell dimensions of initial synthetic H-$(Ni,Fe)_3S_4$ are larger than those reported for D-$(Ni,Fe)_3S_4$, however after annealing they are in excellent agreement.[9,49] The unit cell dimensions are mostly determined by the metal−sulfur bond length,[10] and the initial large value may indicate a metastable state for H-$(Ni,Fe)_3S_4$, with annealing resulting in some compositional readjustment or metal ordering. No significant differences in cell dimensions were observed for the annealed samples after laboratory storage for 6 months.

The Scherrer crystallite size increases upon annealing. The size of H-$Fe_{1.19}Ni_{1.77}S_4$ is 18 ± 2 nm, much smaller than the precursor $Fe_{4.60}Ni_{4.55}S_8$ crystallite size, 67 ± 3 nm. The H-$Fe_{1.19}Ni_{1.77}S_4$ crystallite size increases to 32 ± 2 nm after annealing for 3 days at 300 °C. Prolonged annealing for up to 33 days only increases the size to 38 ± 3 nm (Figure 5). The increased size indicates a recrystallization process, but this process does not proceed at a significant rate at room temperature, as no coarsening was observed after 6 months laboratory storage. This is consistent with nature as natural violarite is always relatively fine grained.[50]

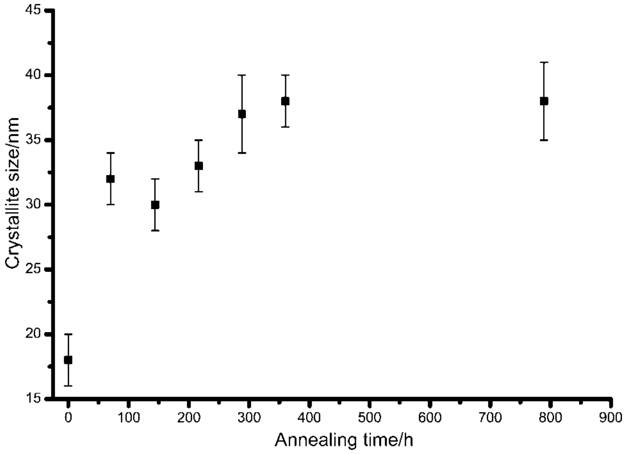

Figure 5. H-$Fe_{1.19}Ni_{1.77}S_4$ crystallite size versus further annealing at 300 °C.

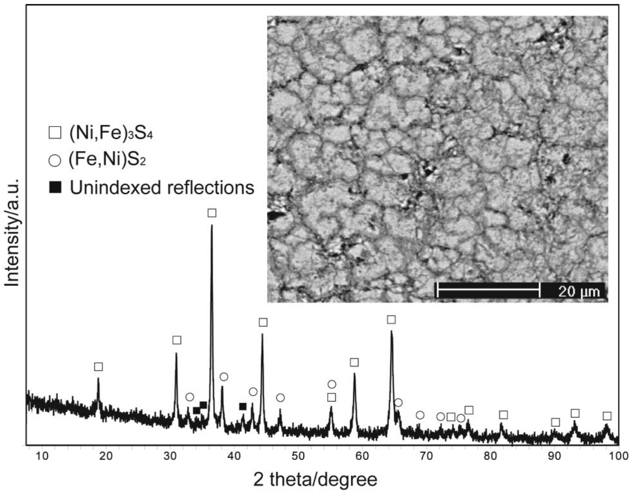

Figure 6. X-ray diffraction pattern and backscattered electron image of H-$(Ni,Fe)_3S_4$ from reaction HV2 (Table 2) after further annealing at 300 °C for 33 days.

Although violarite was reported to have a maximum thermal stability of 461 ± 3 °C,[9] annealing at 300 °C led to the appearance of small amounts of nickeliferous pyrite $(Fe,Ni)S_2$ and some unknown phase(s) with X-ray diffraction lines at d ~2.535, ~2.981, and ~3.053 Å (Figure 6). From mass balance considerations, these reflections probably belong to metal rich phase(s) with compositions similar to *mss* or ferroan millerite ((Ni,Fe)S).

3.4. Hydrothermal versus Dry Synthesis of D-$(Ni,Fe)_3S_4$. Details of the starting compositions, stoichiometries, unit cell dimensions, and purity of the synthetic D-$(Ni,Fe)_3S_4$, as well as the other phases detected in the final product are summarized in Table 3. Note that the compositions determined by electron microprobe analyses are significantly

---

(48) Nickel, E. H. In *Australia I.M.M. Conference*; Australia Institute of Mining and Metallurgy: Parkville, Australia, 1973; pp 111–116.

(49) Richardson, S.; Vaughan, D. J. *Mineral. Mag.* **1989**, *53*, 213–222.

(50) Misra, K. C.; Fleet, M. E. *Econ. Geol.* **1974**, *69*, 391–403.

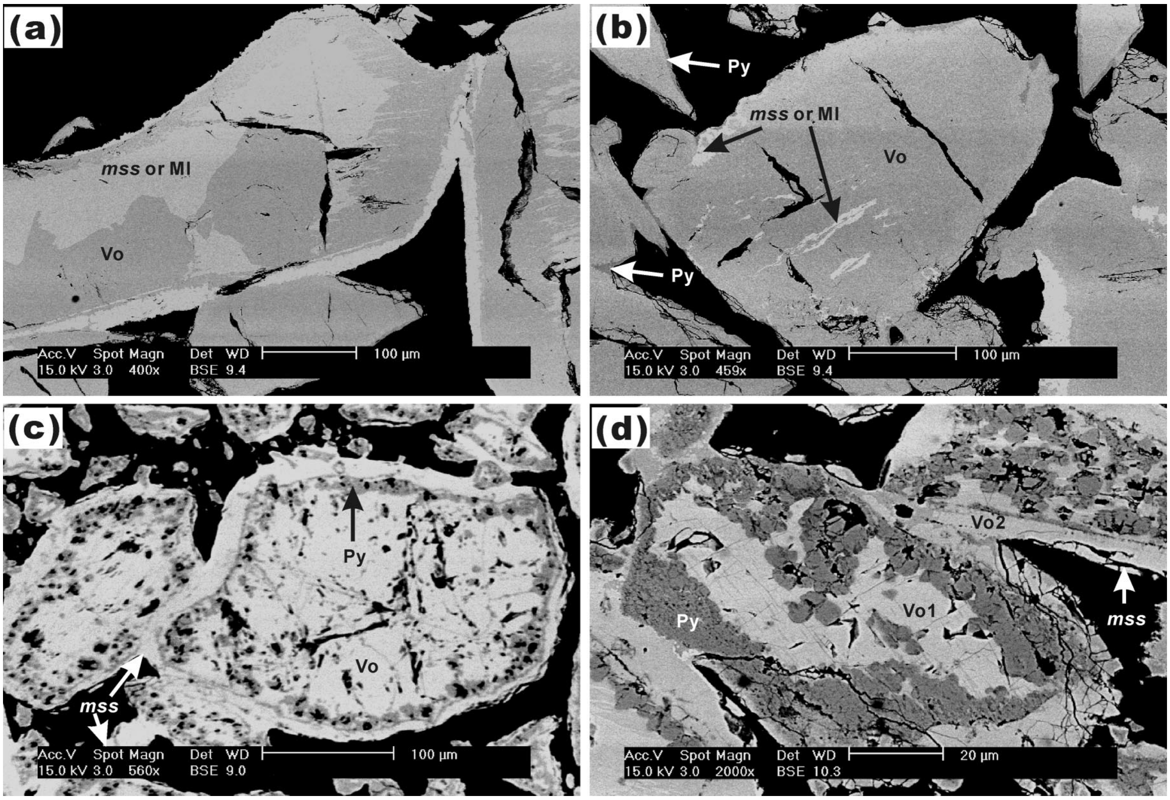

Figure 7. Backscattered electron (BSE) micrographs of synthetic D-$(Ni,Fe)_3S_4$ using starting composition of (a) DV1, (b) DV2, (c) DV3, and (d) DV4 (see Table 3). Vo stands for $(Ni,Fe)_3S_4$, *mss* for (Ni,Fe)S (space group $P6_3/mmc$), Ml for (Ni,Fe)S (space group $R3m$), and Py for $(Fe,Ni)S_2$.

different from the ideal stoichiometries given in section 2.2. This is a reflection of the high levels of impurities in the D-$(Ni,Fe)_3S_4$. The cell dimensions of samples DV1 and DV2 are similar to that of the 300 °C annealed H-$(Ni,Fe)_3S_4$ and those reported by previous workers.[9,49] The Scherrer crystallite size of D-$(Ni,Fe)_3S_4$ is around 50 nm, somewhat larger than that of H-$(Ni,Fe)_3S_4$, but even after annealing at 300 °C for 20 + 80 days, the D-$(Ni,Fe)_3S_4$still contains levels of significant impurities. These impurities were detected by XRD, and also imaged by SEM (Figure 7).

The impurities for the nickel-rich composition are principally nickel-rich *mss* and ferroan millerite ((Ni,Fe)S). The ferroan millerite produced via a phase transition from nickel-rich *mss,* very similar to the phase transition of iron-free phases from α-NiS to β-NiS.[51,52] The purity of the nickel-rich sample DV1 is only 70 ± 3 wt %. In DV2, apart from nickel-rich *mss* and ferroan millerite (Ni,Fe)S, a small amount of nickeliferous pyrite $(Fe,Ni)S_2$ was also detected. The overall purity of DV2 was 73 ± 3 wt %, the highest yield in the current study. Tenailleau et al. obtained a similar value of 76 wt %.[10] Iron-rich D-$(Ni,Fe)_3S_4$ has not been reported in the literature and is believed to be metastable from bonding models.[31] This work indicates that it can be synthesized (DV3 and DV4), but with higher levels of impurities than the ideal or Ni-rich compositions (DV1 and DV2): the purities are 62 ± 3 wt % for DV3, and 54 ± 3 wt % for DV4. Note that the most Fe-rich composition (DV4) suffered phase separation into two D-$(Ni,Fe)_3S_4$ compositions (Vo1 and Vo2): one Fe-rich and the other Ni-rich. In the Fe-rich D-$(Ni,Fe)_3S_4$, the most common impurity is nickeliferous pyrite $(Fe,Ni)S_2$.

The H-$(Ni,Fe)_3S_4$ annealing experiments and the D-$(Ni,Fe)_3S_4$ synthesis, indicate that violarite actually decomposes at or below 300 °C. This is the reason for the difficulty of synthesing pure violarite under dry conditions. However, decreasing the synthesis temperature would require a longer annealing time.

3.5. Synthesis of Co_3S_4. Linnaeite (Co_3S_4) is another thiospinel, but has much higher thermal stability than $(Ni,Fe)_3S_4$. The decomposition temperature of Co_3S_4 is 664 °C,[53] thus it is relatively easy to synthesize via the traditional dry condition method,[33,54] although the purity of the product was not reported. We succeeded in producing Co_3S_4 via a replacement reaction using the precursor Co_9S_8 (see details in Tables 1 and 2). The refined unit cell of the precursor is in excellent agreement with literature values.[55,56]

The partially replaced grain shown in Figure 8 shares all the features of the transformation of $(Fe,Ni)_9S_8$ to H-$(Ni,Fe)_3S_4$, indicating a common coupled dissolution−reprecipitation mechanism. One difference is that the synthetic Co_3S_4 is significantly metal-deficient: the Co/S ratio is 0.688 compared to the ideal Co/S ratio 0.75.

---

(51) Kullerud, G.; Yund, R. A. *J. Petrol.* **1962**, *3*, 126–175.
(52) Wang, H.; Pring, A.; Ngothai, Y.; O'Neill, B. *Am. Mineral.* **2006**, *91*, 171–181.
(53) Kullerud, G. *Carnegie Inst. Wash., Ann. Rep.* **1968**, *67*, 179–182.
(54) Bouchard, R. J.; Russo, P. A.; Wold, A. *Inorg. Chem.* **1965**, *4*, 685–688.
(55) Kitakaze, A.; Sugaki, A. *Can. Mineral.* **2004**, *42*, 17–42.
(56) Kaneda, H.; Takenouchi, S.; Shoji, T. *Miner. Deposita* **1986**, *21*, 161–180.

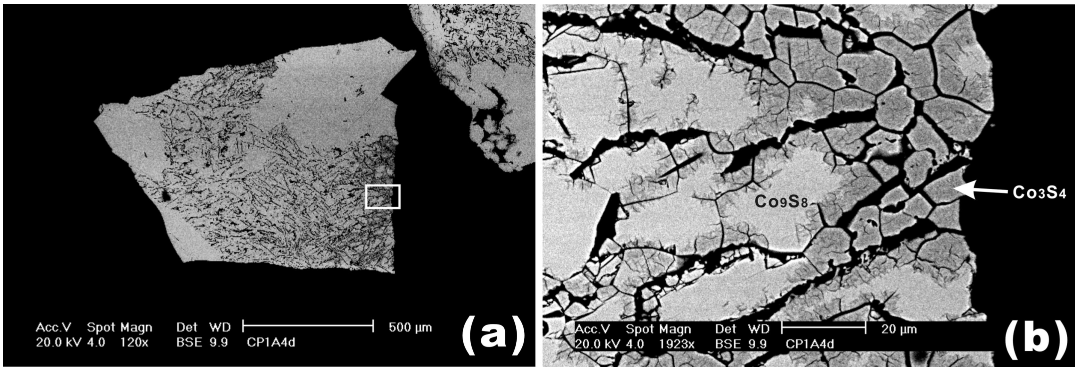

Figure 8. Backscattered electron (BSE) micrographs of partially replaced Co_9S_8 at 125 °C and pH 3.90. Image (b) is the enlargement of the write box drawn in image (a).

4. Conclusions

The complex sulfide, $(Ni,Fe)_3S_4$, has been successfully prepared via a coupled dissolution−reprecipitation pathway using a hydrothermal flow-through cell. The composition of $(Ni,Fe)_3S_4$ can be adjusted across a wide range of Fe/Ni ratios by varying the reaction conditions (e.g., temperature, pH) and the composition of the corresponding precursors. The precursors need to be pure and relatively easy to synthesize, but minor reactive impurities in the precursors do not affect the purity of the final products. The synthesis is much faster via this route than the traditional dry synthesis, and the $(Ni,Fe)_3S_4$ products have higher purity. The fluid flow improves the purity as it flushes away the insoluble Fe_2O_3 byproduct during the reaction.

Although the dissolution−reprecipitation route is most suitable to prepare sulfides with low thermal stabilities, it can also be used to synthesize sulfides with high thermal stabilities. As an example, Co_3S_4 (stable to 664 °C) has also been successfully synthesized.

The reactions studied here are redox reactions, and the oxidant used was aqueous oxygen. The air reservoir needed to be refreshed at regular intervals to sustain the reaction. Thus it is crucial to find a suitable oxidant that can be introduced to support the reaction to completion, without affecting the thermodynamic stability of the phases being synthesized.

Considering the pseudomorphic nature of dissolution−reprecipitation reactions, we can expect a further advantage of this method: the morphology, texture, and orientation of the products can be tuned and optimized to meet specific requirements and suit particular applications by controlling the corresponding parameters of the precursors.

Acknowledgment. The current work is funded by an Australian Research Council Project (DP0772299). Adelaide Microscopy Center staff Mr, John Terlet, Dr. Peter Self, Mr. Angus Netting, and Ms. Lyn Waterhouse are gratefully acknowledged for their assistance in using the FESEM and EMP. Chemical Engineering Workshop (Adelaide University) staff Jason Peak and Brian Mulcahy are thanked for building up and maintaining the hydrothermal flow-through cell. We also thank the editor and the anonymous referees for their constructive suggestions for the improvement of the manuscript. F.X. thanks the Department of Education, Science and Training, Australian Government, for the EIPRS scholarship, which has enabled his participation in this project.

CM7033883